Science Advances
AAAS

advances.sciencemag.org/cgi/content/full/6/17/eaba3252/DC1

Supplementary Materials for

Wireless smart contact lens for diabetic diagnosis and therapy

Do Hee Keum, Su-Kyoung Kim, Jahyun Koo, Geon-Hui Lee, Cheonhoo Jeon, Jee Won Mok, Beom Ho Mun, Keon Jae Lee, Ehsan Kamrani, Choun-Ki Joo, Sangbaie Shin, Jae-Yoon Sim, David Myung, Seok Hyun Yun, Zhenan Bao, Sei Kwang Hahn*

*Corresponding author. Email: skhanb@postech.ac.kr

Published 24 April 2020, *Sci. Adv.* **6**, eaba3252 (2020)
DOI: 10.1126/sciadv.aba3252

The PDF file includes:

Other Supplementary Material for this manuscript includes the following:

(available at advances.sciencemag.org/cgi/content/full/6/17/eaba3252/DC1)

Supplementary Figures

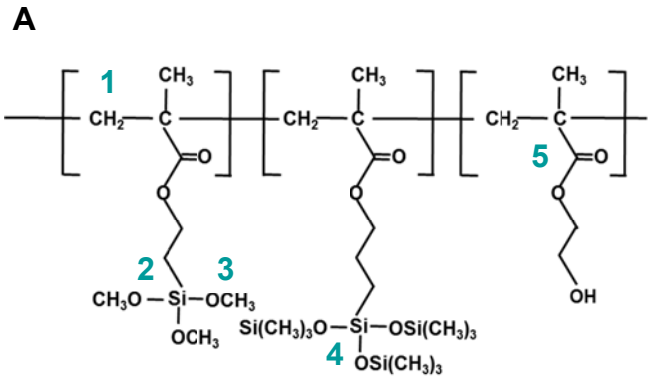

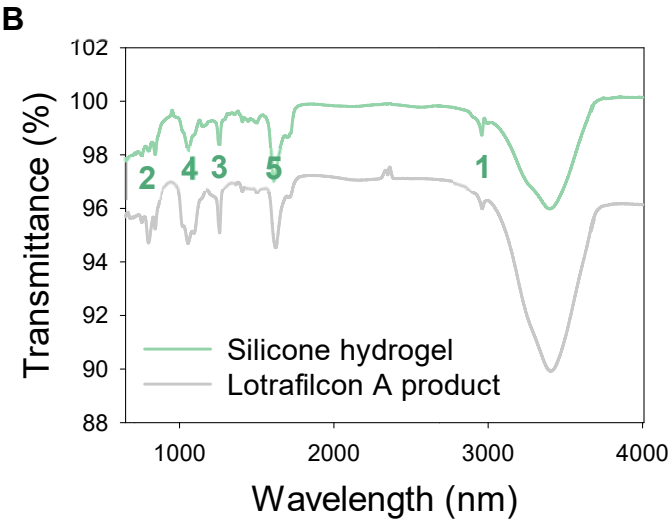

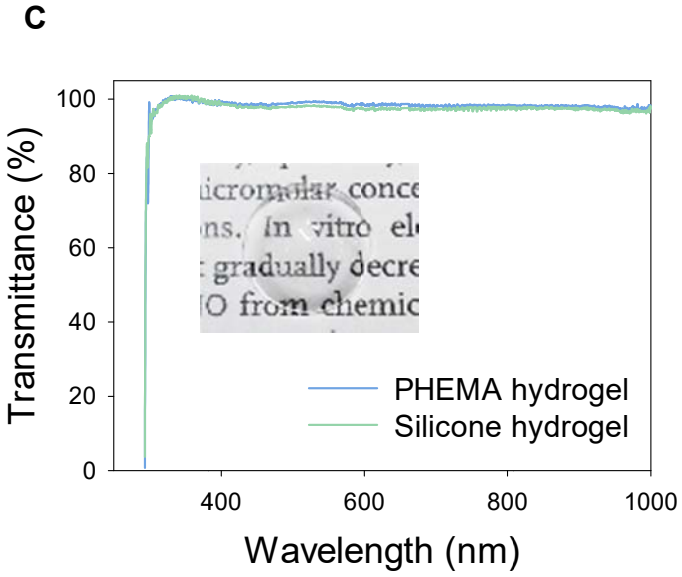

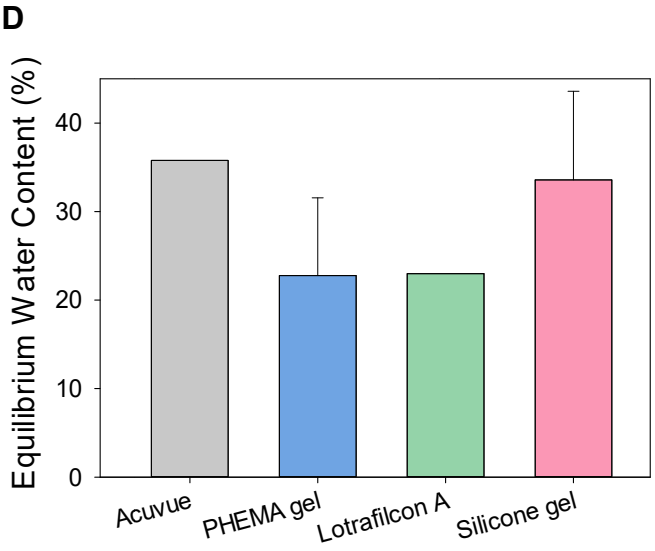

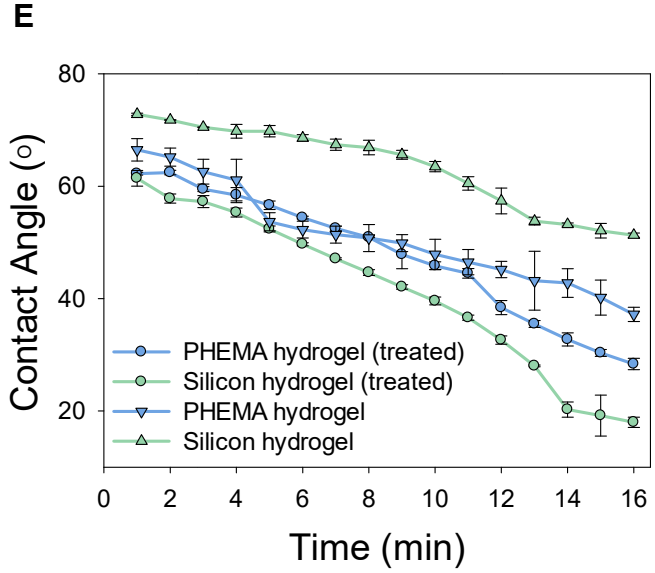

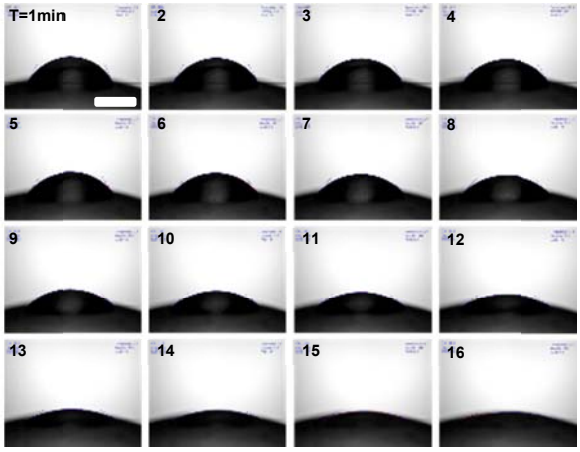

Fig. S1. Characterization of contact lens materials. (**A**) Chemical structure of crosslinked silicone hydrogels for smart contact lens. (**B**) Attenuated total reflectance - Fourier transform infrared spectroscopy (ATR-FTIR) of silicone hydrogel contact lens and Lotrafilcon A. **(C)** Transmittance spectrum of silicone hydrogel and poly(2-hydroxyethyl methacrylate) (PHEMA) hydrogel contact lenses. A photograph of silicone hydrogel contact lens on the text showing the visual clarity. **(D)** The equilibrium water content of Acuvue lens, PHEMA contact lens, Lotrafilcon A, and silicone hydrogel contact lens (n = 6). (**E**) The comparison of water contact angles between PHEMA and silicone hydrogel contact lenses with increasing time. (**F**) Photographs for the absorption of water droplet on silicone hydrogel contact lens over time (n = 6, scale bar = 0.7 mm).

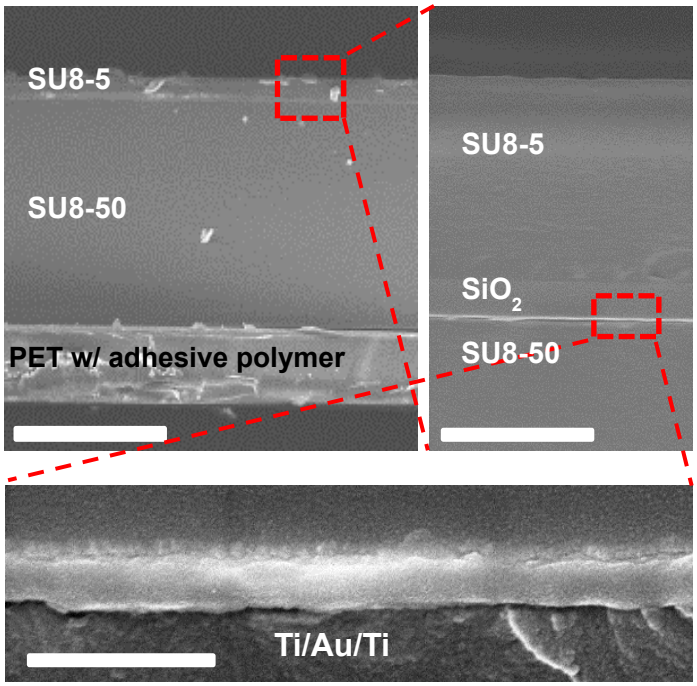

Fig. S2. Cross-sectional electron microscopic images of f-DDS. Scale bars represent 5 μm for left top, 50 μm for right top, and 500 μm for bottom, respectively.

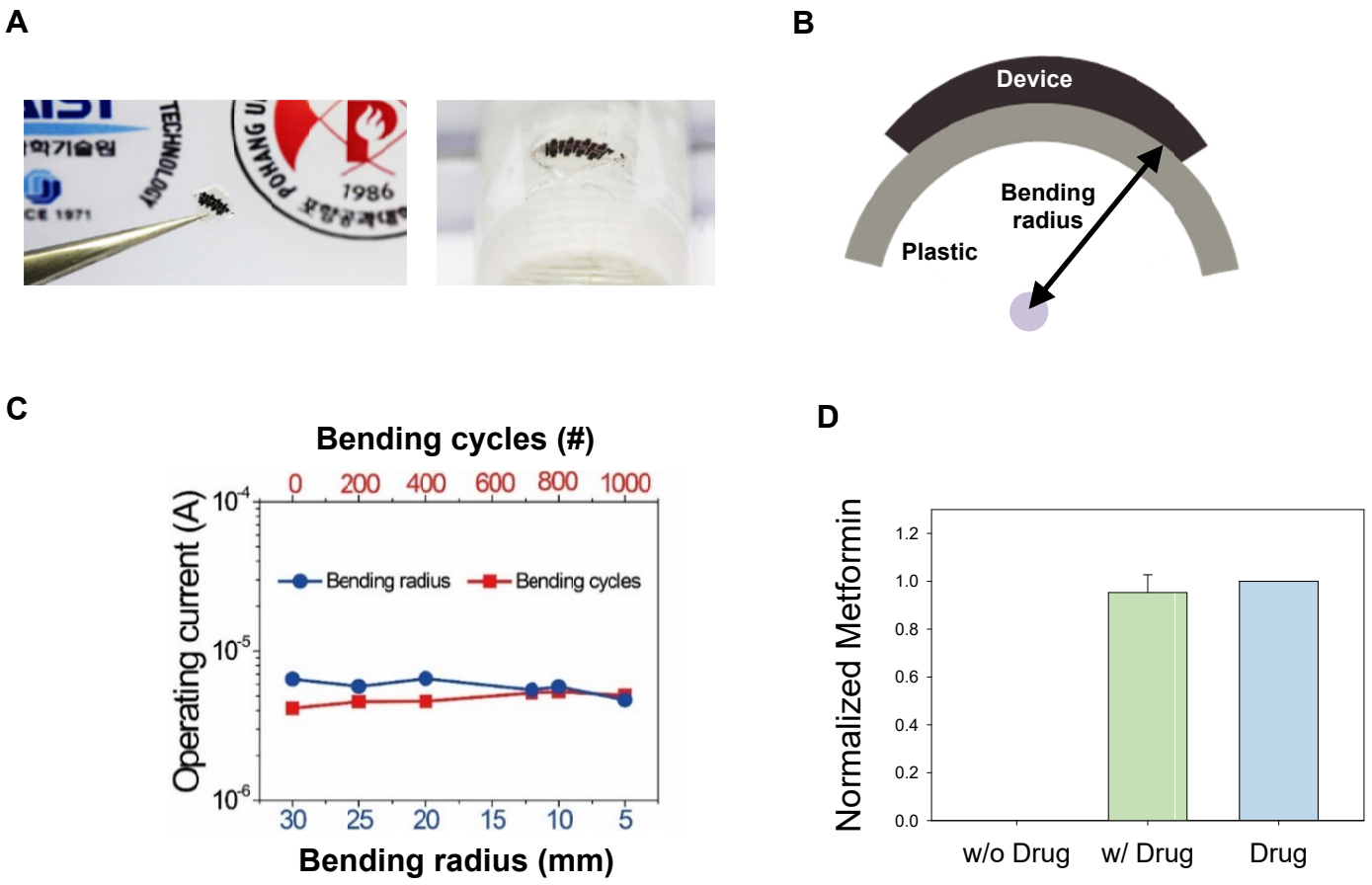

Fig. S3. Bending and in vitro drug release tests of f-DDS. (**A**) The photograph of flexible drug delivery system (f-DDS) wrapped on polydimethylsiloxane (PDMS) rod with a radius of 5 mm. Photo credit: Beom Ho Mun, KAIST. (**B**) Schematic illustration for the mechanical bending test. (**C**) Operating current of f-DDS for drug release according to the several bending radius (blue) and the bending cycles (red) in a 5 mm-bended state. (**D**) The released concentration of metformin from the reservoirs (n = 6) in comparison with the loaded content.

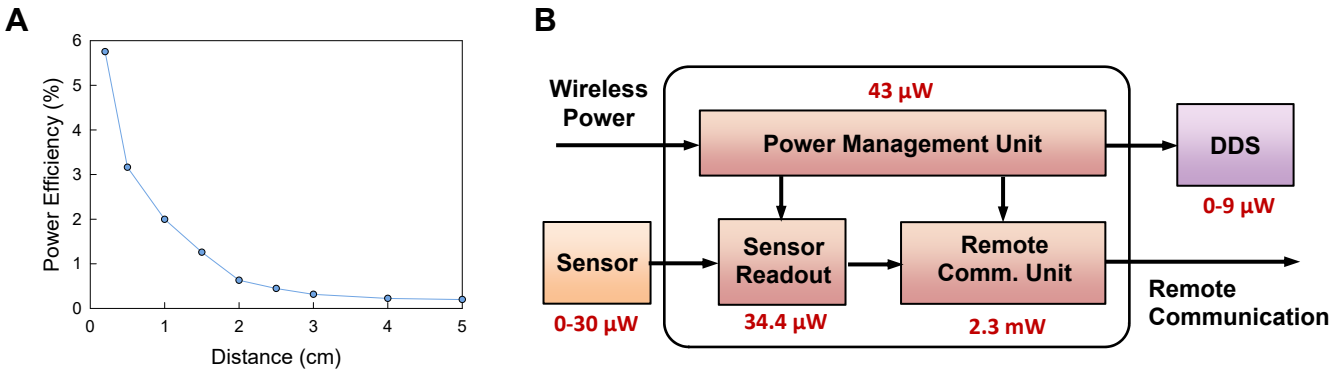

Fig. S4. Wireless power transmission and the power consumption of smart contact lens. (**A**) The power transmission efficiency according to the distance between transmitter and receiver coils. (**B**) A block diagram showing the amount of power consumption in the smart contact lens.

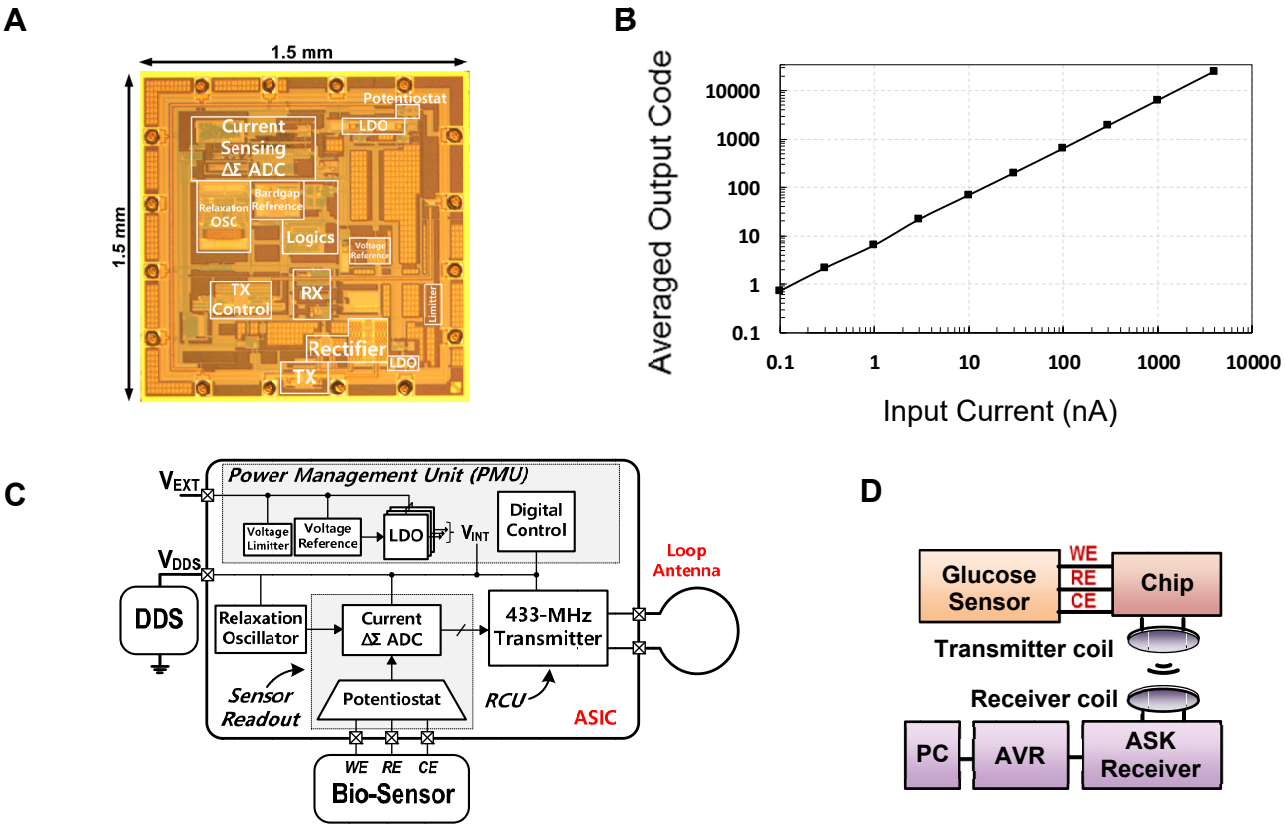

Fig. S5. Schematic illustration for the integrated circuit chip in the smart contact lens. (**A**) Optical microscopic image of the integrated circuit (IC) chip. (**B**) The averaged output code of analogue-to-digital converter (ADC) according to the input current. (**C**) Overall architecture of the ASIC chip. (**D**) Schematic representation of wireless power transmission and remote communication systems.

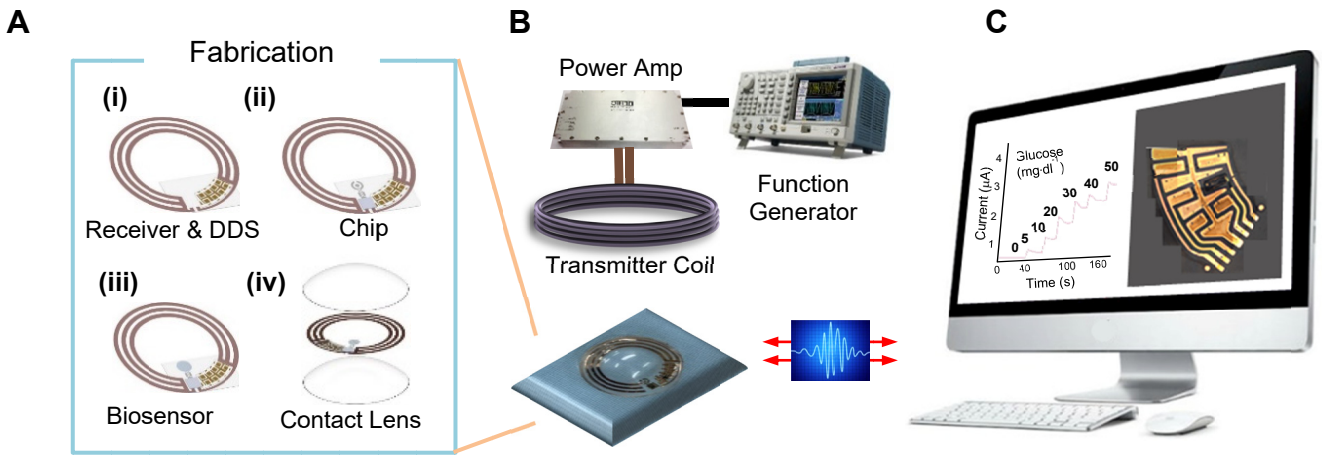

Fig. S6. Schematic illustration for the fabrication and applications of smart contact lens. (**A**) Fabrication of smart contact lens. (i) The attachment of power receiver coil with flexible drug delivery system (f-DDS) on poly(ethylene terephthalate) (PET) substrate. (ii) The deposition of biosensor electrodes and the electrical connection of the integrated circuit chip with the power receiver coil, f-DDS and biosensor. (iii) The coating of glucose sensing channel for biosensor. (iv) The molding of integrated devices in silicone contact lens materials. (**B**) The wireless power transmission and remote communication system of smart contact lens. (**C**) The wirelessly delivered data from the glucose biosensor and the state of drug reservoirs shown on a PC monitor in real-time.

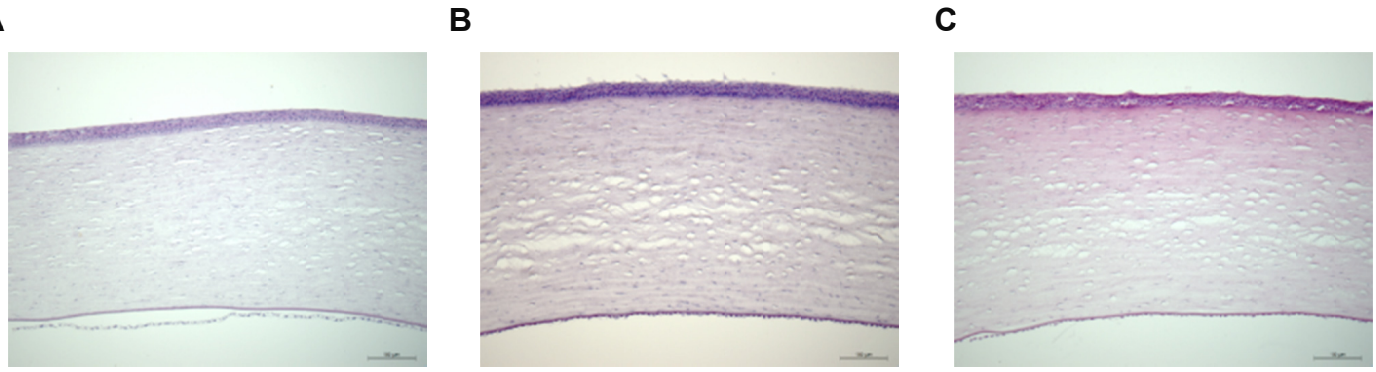

Fig. S7. Histological analysis of corneas in the eyes of New Zealand white rabbits. (**A**) Without smart contact lens (normal), and with smart contact lens for (**B**) 3 and (**C**) 5 days (scale bar = 0.1 mm

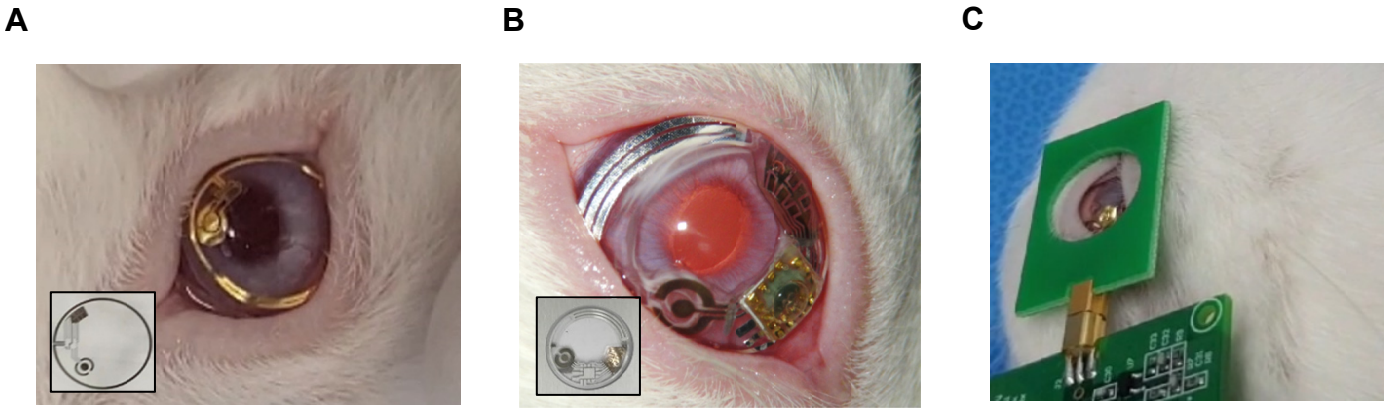

Fig. S8. Photo-images for integrated smart contact lens and wireless power transmission *in vivo*. The photo-image of a rabbit eye wearing (**A**) the integrated smart contact lens for only glucose sensing and (**B**) the integrated smart contact lens for both glucose sensing and drug delivery, and (**C**) wireless power transmission systems using an external transmission coil and a receiver coil on the smart contact lens. Photo credit: Su-Kyoung Kim and Do Hee Keum, POSTECH.

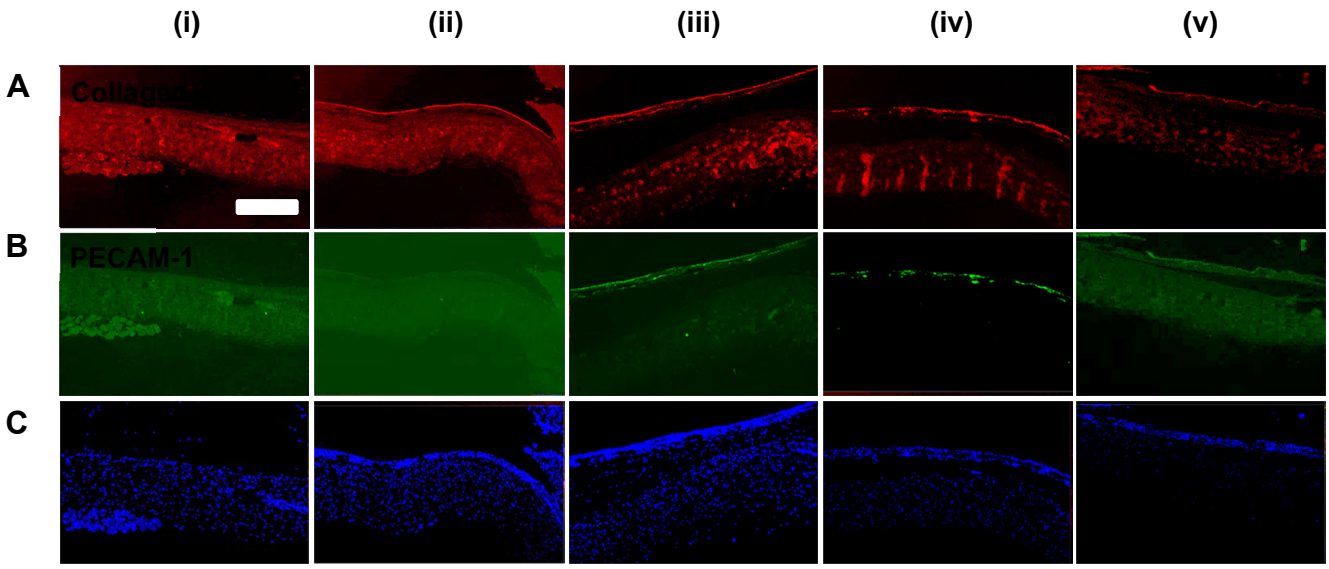

Fig. S9. Immunohistochemical analysis for diabetic retinopathy therapy. Immunohistochemical staining images for (**A**) collagen type 4 in red and (**B**) platelet EC adhesion molecule-1 (PECAM-1) in green. (**C**) Nuclear staining by 4',6-diamidine-2'-phenylindole dihydrochloride (DAPI) in blue (scale bar = 0.1 mm). Diabetic retinas of rabbits were treated with (i) eye-drop of phosphate buffer saline (negative control), (ii) eye-drop of genistein, (iii) intravitreal injection of genistein, (iv) intravitreal injection of Avastin (positive control), and (v) smart contact lens.

Movie S1. In vivo applications of smart contact lens on diabetic rabbit eyes.